Electronic Supplementary Information

Regulation of Backbone Structure and Optoelectrical Properties of Bis-Pyridal[2,1,3]thiadiazole-Based Ambipolar Semiconducting Polymers via a Fluorination Strategy

Xin Tao,‡[a] Yanwei Liu,‡[b] Lulu Du,[a] Yongkun Yan,[c] Zeng Wu,[c] Yan Zhao,*[c] Yunlong Guo,*[b] Huajie Chen,*[a] Yunqi Liu[b,c]

[1]*Key Laboratory of Environmentally Friendly Chemistry and Applications of Ministry of Education, College of Chemistry, Xiangtan University, Xiangtan 411105, China. E-mail: chenhjoe@163.com*

[2]*Beijing National Laboratory for Molecular Sciences, Chinese Academy of Sciences, Beijing 100190, China. E-mail: guoyunlong@iccas.ac.cn*

[3]*Laboratory of Molecular Materials and Devices, Department of Materials Science, Fudan University, Shanghai 200438, China. E-mail: zhaoy@fudan.edu.cn*

S1. Instruments

^{1}H, ^{13}C, and ^{19}F NMR spectra were collected on Bruker AVANCE 400 instrument (400 MHz) by using tetramethylsilane (TMS) as the internal standard. Ultraviolet-visible-Near Infrared (UV-vis-NIR) absorption spectra in chlorobenzene (1×10^{-5} M) and as thin films casted on the quartz glass were measured on a Perkin-Elmer lamada 25 spectrophotometer. Mass Spectrometry (MALDI-TOF-MS) was measured on a Bruker Autoflex III instrument. On the basis of a conventional three-electrode electrochemical cell, the oxidation and reduction potentials of both polymers were determined by using a cyclic voltammetry (CV) method on an electrochemistry workstation (CHI660e, Chenhua shanghai). The electrochemical cell includes a Pt wire counter electrode, an Ag/AgCl (KCl, Sat'd) reference electrode, and a Pt working electrode deposited a layer of polymer thin films. The supporting electrolyte is an anhydrous and N_2 saturated acetonitrile solution containing 0.1 M tetrabutylammonium hexafluorophosphate ($TBAPF_6$). Thermogravimetric analysis (TGA) was recorded on Perkin-Elmer TGA-7 with a heating rate of 10 °C min^{-1} under N_2 atmosphere. Differential scanning calorimetry (DSC) was record on a DSC-Q10 with a heating and cooling rate of 20 °C min^{-1} under N_2 atmosphere. A Polymer Labs PL 220 system was adopted to determine the molecular weight

of both polymers at 150 °C in 1,2,4-trichlorobenzene. The molecular weight was calibrated against monodisperse polystyrene standard. Atomic force microscopy (AFM) measurements of the polymer thin films deposited on the glass substrates were collected on a Bruker Multi-Mode 8 microscope using a tapping mode. The microstructure of the polymer thin films deposited on the glass substrates were characterized by the grazing incidence X-ray diffraction (GIXRD) experiments. The molecular geometries and electronic energy levels of the model molecules were calculated via density functional theory (DFT) calculations at the level of B3LYP/6-31G (d). By using graphite-monochromated Cu K Kα radiation (λ = 1.54184 Å), single-crystal X-ray experiments were recorded on a SuperNova, Dual, Cu at zero, AtlasS2 diffractometer. The crystal diagram and related parameters were drawn by Diamond and Mercury. Using Olex2, the structures were solved with the ShelXS structure solution program using Direct Methods and refined with the ShelXL refinement package using Least Squares minimisation.

S2. Gel Permeation Chromatography

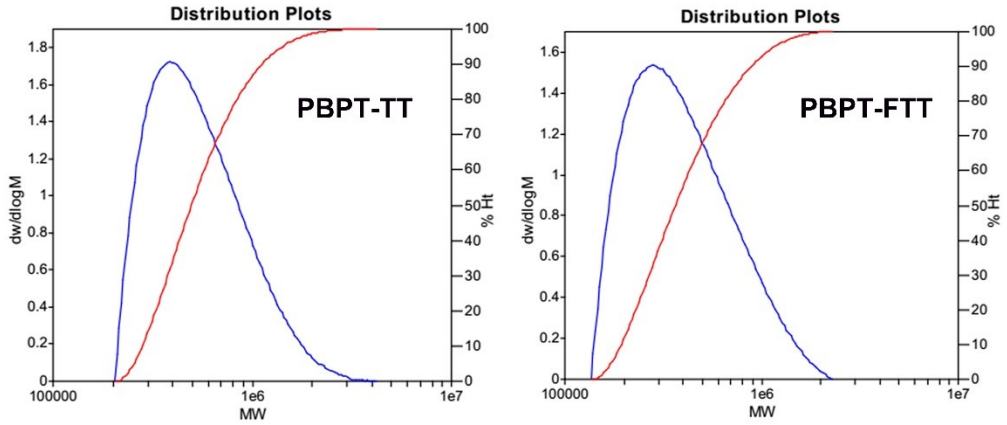

Fig. S1. GPC curves of **PBPT-TT** and **PBPT-FTT**.

S3. Thermogravimetric Analysis

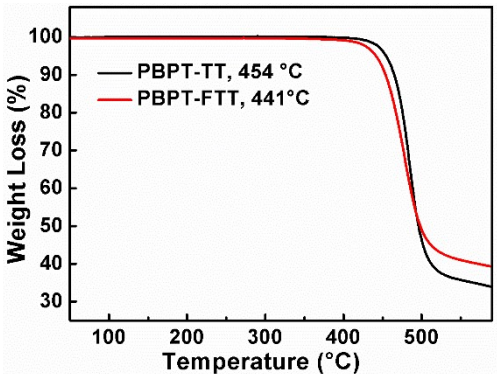

Fig. S2.TGA curves of **PBPT-TT** and **PBPT-FTT**.

Table S1. Crystal Data and Structure Refinement for **BPT-T-1** (CCDC, 2015132).

Identification code	**BPT-T-1**
Empirical formula	$C_{26}H_{24}N_6S_4$
Formula weight	548.75
Temperature/K	100.00 (10)
Crystal system	triclinic
Space group	P-1
a/Å	7.7842 (8)
b/Å	9.3195 (13)
c/Å	17.744 (2)
α/°	98.352 (12)
β/°	101.629 (10)
γ/°	94.886 (10)
Volume/Å^3	1238.7 (3)
Z	2
ρ_{calc}g/cm^3	1.471
μ/mm^{-1}	3.757
F(000)	572.0
Crystal size/mm^3	0.12 × 0.11 × 0.08
Radiation	CuKα (λ = 1.54184)
2Θ range for data collection/°	5.156 to 148.022
Index ranges	$-9 \le h \le 9$, $-9 \le k \le 11$, $-21 \le l \le 20$
Reflections collected	7627
Independent reflections	4750 [R_{int} = 0.0990, R_{sigma} = 0.1194]
Data/restraints/parameters	4750/0/327
Goodness-of-fit on F^2	1.006
Final R indexes [I>=2σ (I)]	R_1 = 0.0893, wR_2 = 0.1676
Final R indexes [all data]	R_1 = 0.0910, wR_2 = 0.1802
Largest diff. peak/hole / e Å^{-3}	1.14/-0.95

S4. Crystal Structure

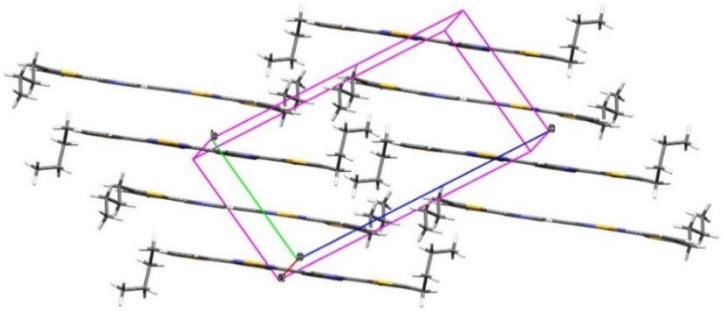

Fig. S3. The crystal packing structure of **BPT-T-1**.

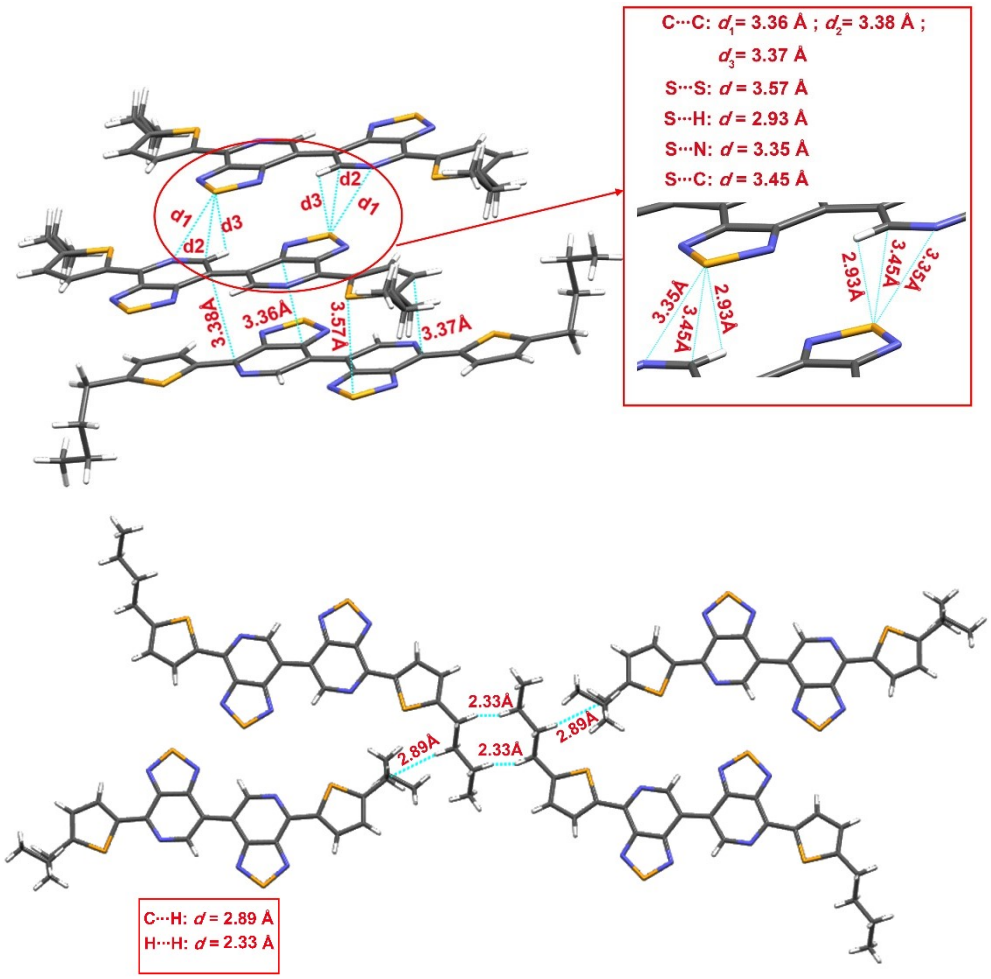

Fig. S4. Crystal organization involves multiple weak interactions, including 1) two C···C interactions ($d_{C\cdots C}$ = 3.36 and 3.38 Å) between the two adjacent **PT** units, 2) one C···C interaction ($d_{C\cdots C}$ = 3.37 Å) and one S···S interaction ($d_{S\cdots S}$ = 3.57 Å) between the PT unit and the adjacent thiophene unit, 3) three types of dispersion interactions between the two adjacent **PT** units ($d_{S\cdots H}$ = 2.93 Å, $d_{S\cdots N}$ = 3.35 Å, and $d_{S\cdots C}$ = 3.45 Å), 4) two types of alkyl chain interactions ($d_{C\cdots H}$ = 2.89 Å, and $d_{H\cdots H}$ = 2.33 Å).

S5. Charge Carrier Transport Performance.

Table S2. Electrical characteristics of the OFETs based on the **PBPT-TT** films annealed at different temperatures.

PBPT-TT	Hole Transport			Electron Transport		
	μ_h Max./Avg.[a] ($cm^2\ V^{-1}\ s^{-1}$)	I_{on}/I_{off}	V_{th} (V)	μ_e Max./Avg.[a] ($cm^2\ V^{-1}\ s^{-1}$)	I_{on}/I_{off}	V_{th} (V)
100°C	0.0068 /0.0062	4×10^2	–17	0.0003 /0.0003	1×10^2	75
120°C	0.0073 /0.0069	2×10^2	–17	0.0004 /0.0004	1×10^2	75
140°C	0.0124 /0.0113	4×10^2	–33	0.0049 /0.0045	3×10^2	57
160°C	0.0135 /0.0122	2×10^3	–34	0.0191 /0.0182	5×10^2	72
180°C	0.0064 /0.0052	6×10^2	–33	0.0054 /0.0051	1×10^2	57
200°C	0.0017 /0.0011	2×10^2	–35	0.0057 /0.0053	2×10^2	56

[a]The maximum and average mobilities was obtained from more than 10 devices.

Table S3. Electrical characteristics of the OFETs based on the **PBPT-FTT** films annealed at different temperatures.

PBPT-FTT	Hole Transport			Electron Transport		
	μ_h Max./Avg.[a] ($cm^2\ V^{-1}\ s^{-1}$)	I_{on}/I_{off}	V_{th} (V)	μ_e Max./Avg.[a] ($cm^2\ V^{-1}\ s^{-1}$)	I_{on}/I_{off}	V_{th} (V)
160°C	0.152 /0.145	7×10^3	–43	0.366 /0.384	5×10^4	78
180°C	0.168 /0.163	6×10^3	–42	0.547 /0.962	8×10^4	75
200°C	0.332 /0.289	8×10^3	–36	1.602 /1.519	2×10^5	65
220°C	0.195 /0.181	2×10^4	–33	0.710 /0.680	4×10^4	70
240°C	0.128 /0.113	2×10^3	–30	0.424 /0.402	3×10^4	62

[a]The maximum and average mobilities was obtained from more than 10 devices.

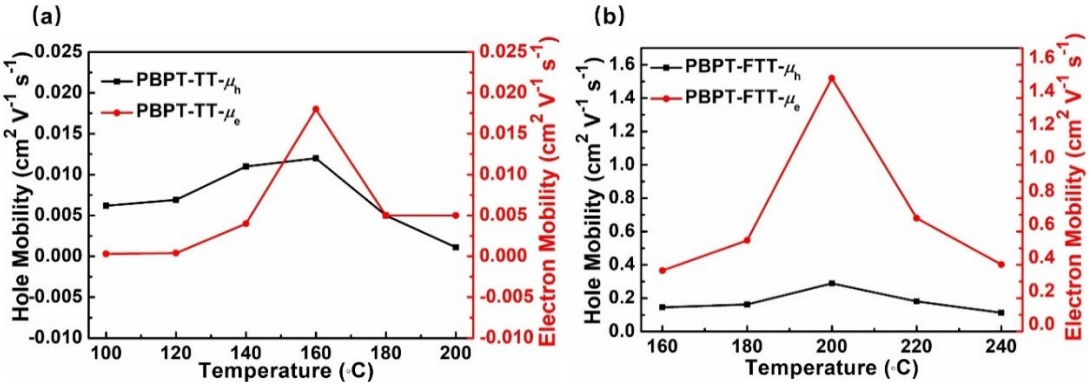

Fig. S5. The relationship between annealing temperatures and mobilities of the OFET devices fabricated from (a) **PBPT-TT** and (b) **PBPT-FTT** films.

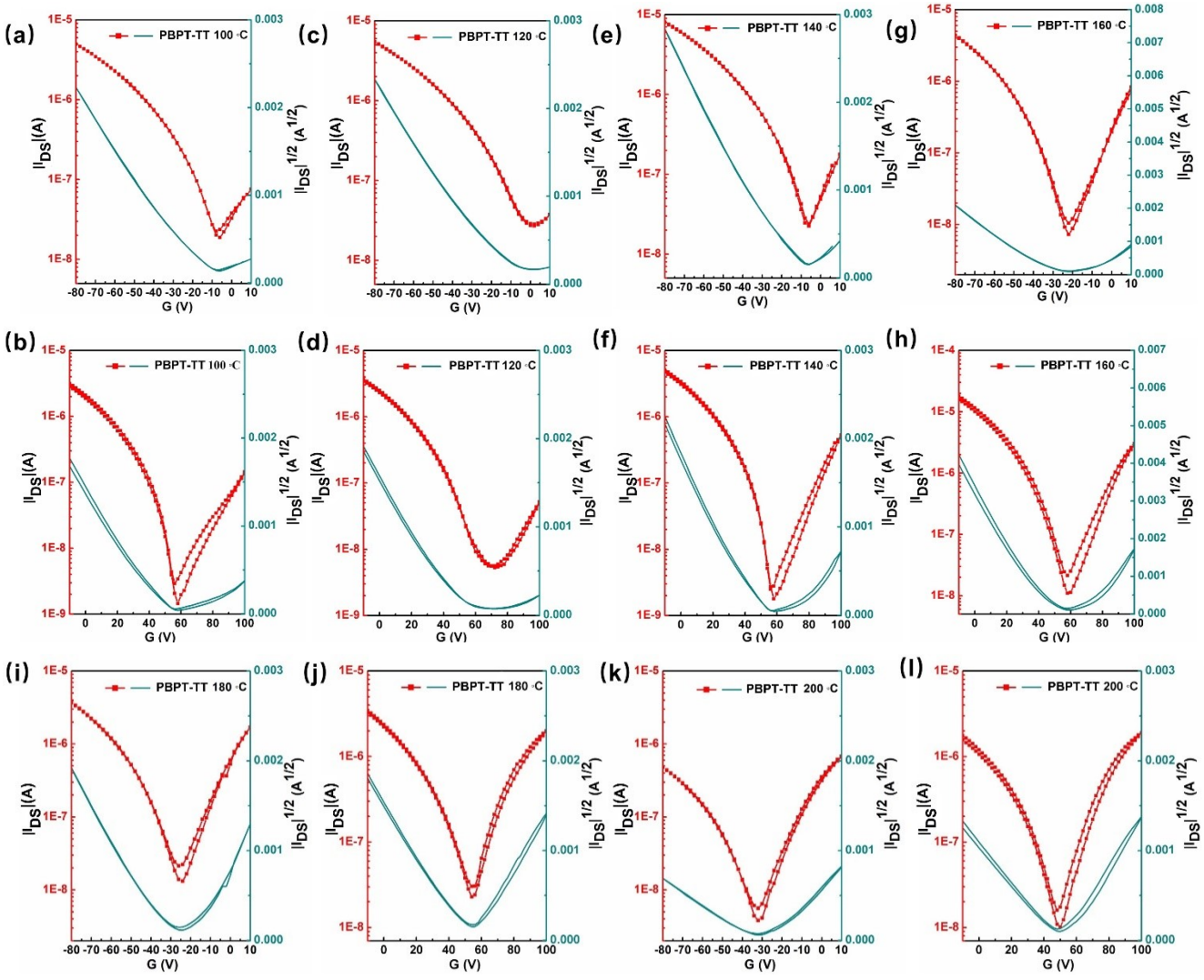

Fig S6. Transfer curves of the OFET device based on the polymer **PBPT-TT** after thermal annealing for 10 min at 100 ℃ (a and b) ,120 ℃ (c and d), 140 ℃ (e and f), 160 ℃ (g and h), 180 ℃ (i and j) and 200 ℃ (k and l), respectively.

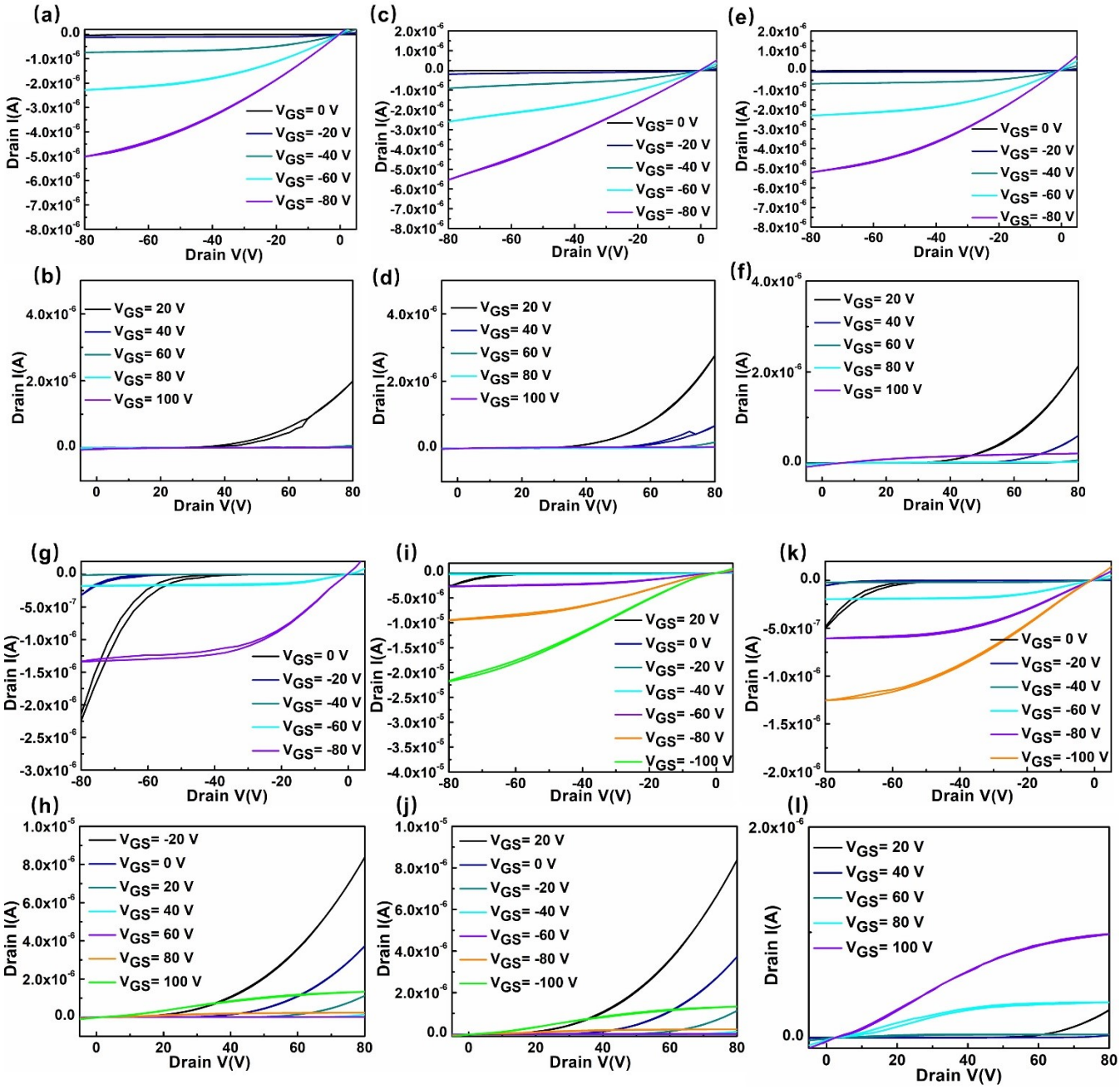

Fig S7. Output curves of the OFET device based on the polymer **PBPT-TT** after thermal annealing for 10 min at 100 ℃ (a and b) ,120 ℃ (c and d), 140 ℃ (e and f), 160 ℃ (g and h), 180 ℃ (i and j) and 200 ℃ (k and l), respectively.

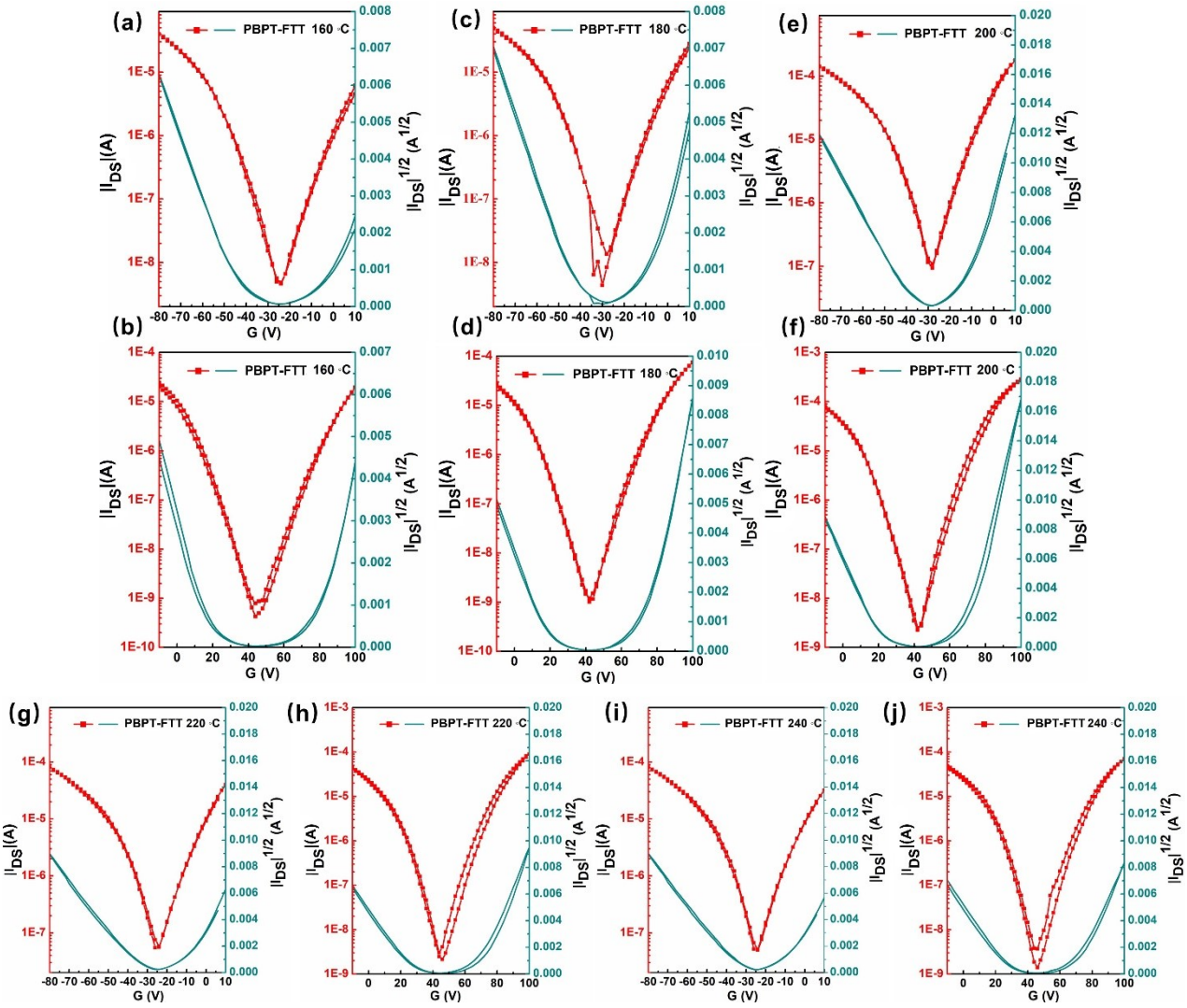

Fig S8. Transfer curves of the OFET device based on the polymer **PBPT-FTT** after thermal annealing at for 10 min 160 ℃ (a and b) ,180 ℃ (c and d), 200 ℃ (e and f), 220 ℃ (g and h), 240 ℃ (i and j), respectively.

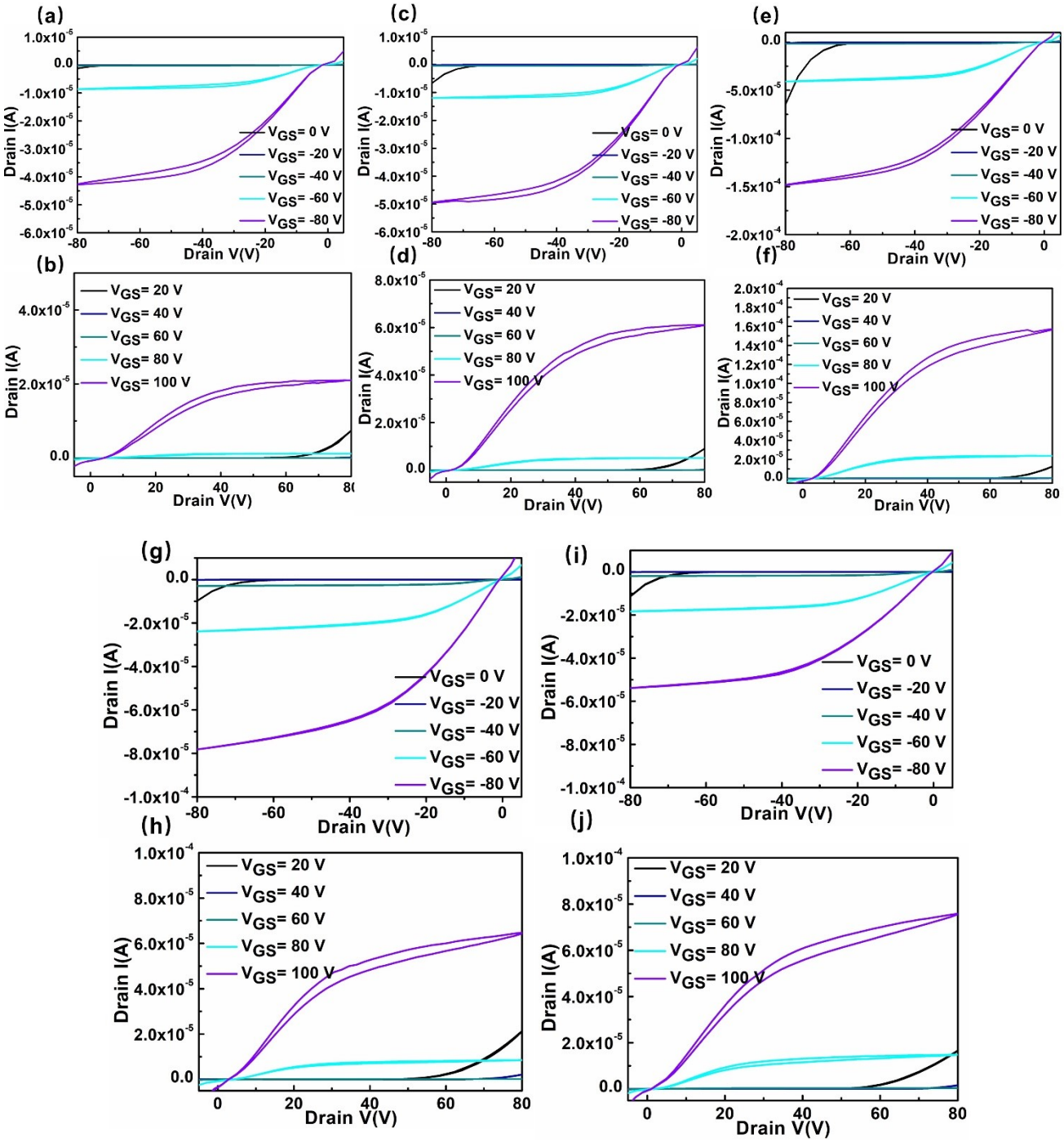

Fig S9. Output curves of the OFET device based on the polymer **PBPT-FTT** after thermal annealing for 10 min 160 ℃ (a and b) ,180 ℃ (c and d), 200 ℃ (e and f), 220 ℃ (g and h), 240 ℃ (i and j), respectively.

Table S4. Crystal coherence lengths and π–π stacking (010) peak centers of both PBPT-TT and PBPT-FTT thin films

Polymer	Orientation	Peak Center ($Å^{-1}$)	FWHM ($Å^{-1}$)	*L* (nm)
PBPT-TT	Face-on	1.75	0.178	3.53
PBPT-FTT	Edge-on	1.84	0.137	4.59

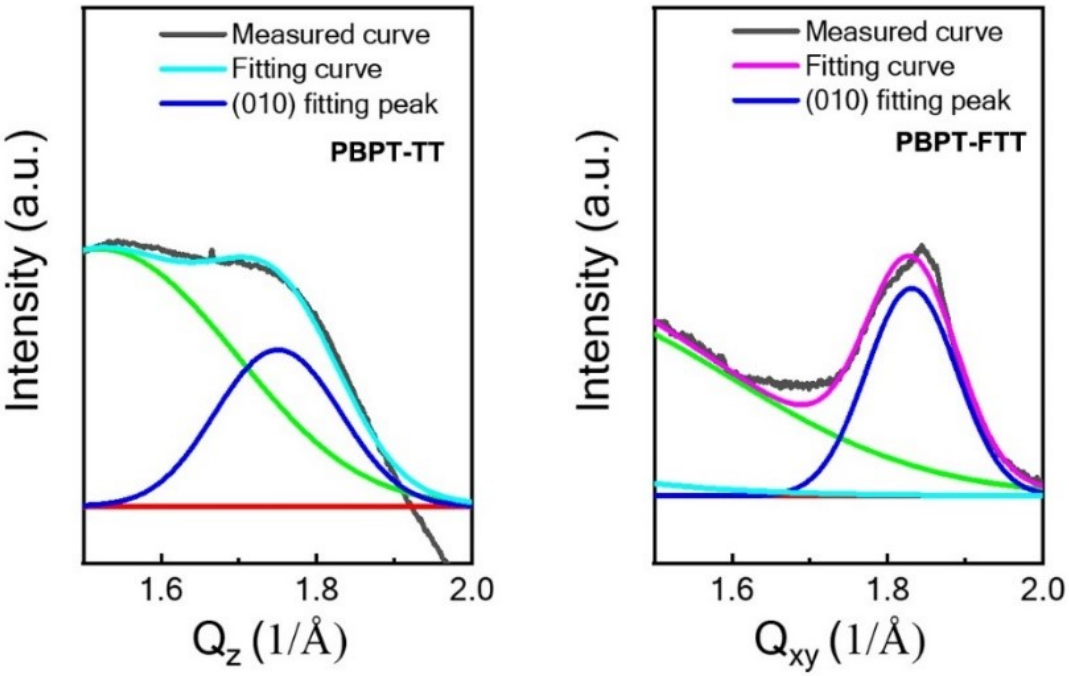

Fig. S10. The FWHM are estimated according to the Gaussian fitted (010) peaks.

S6. ^{1}H NMR and ^{13}C NMR spectra

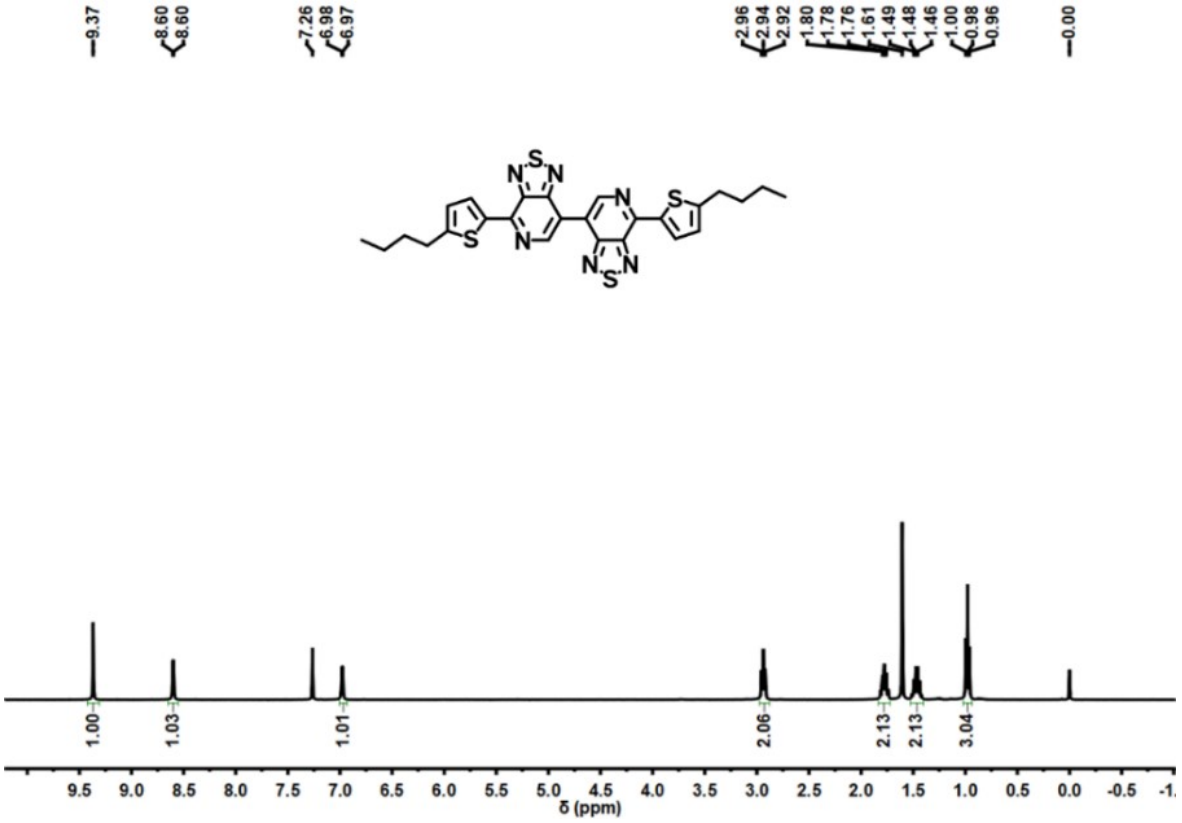

Fig. S11. ^{1}H NMR spectrum of **BPT-T-1** ($CDCl_3$, 25 °C)

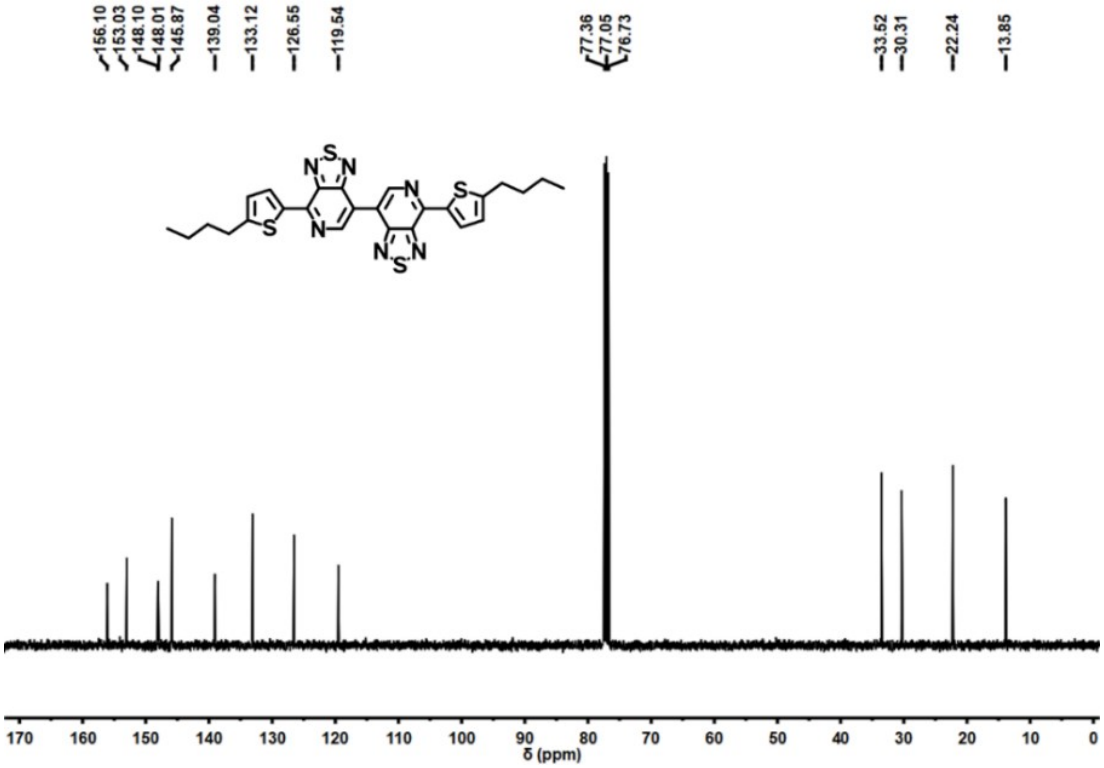

Fig. S12. ^{13}C NMR spectrum of **BPT-T-1** ($CDCl_3$, 25 °C).

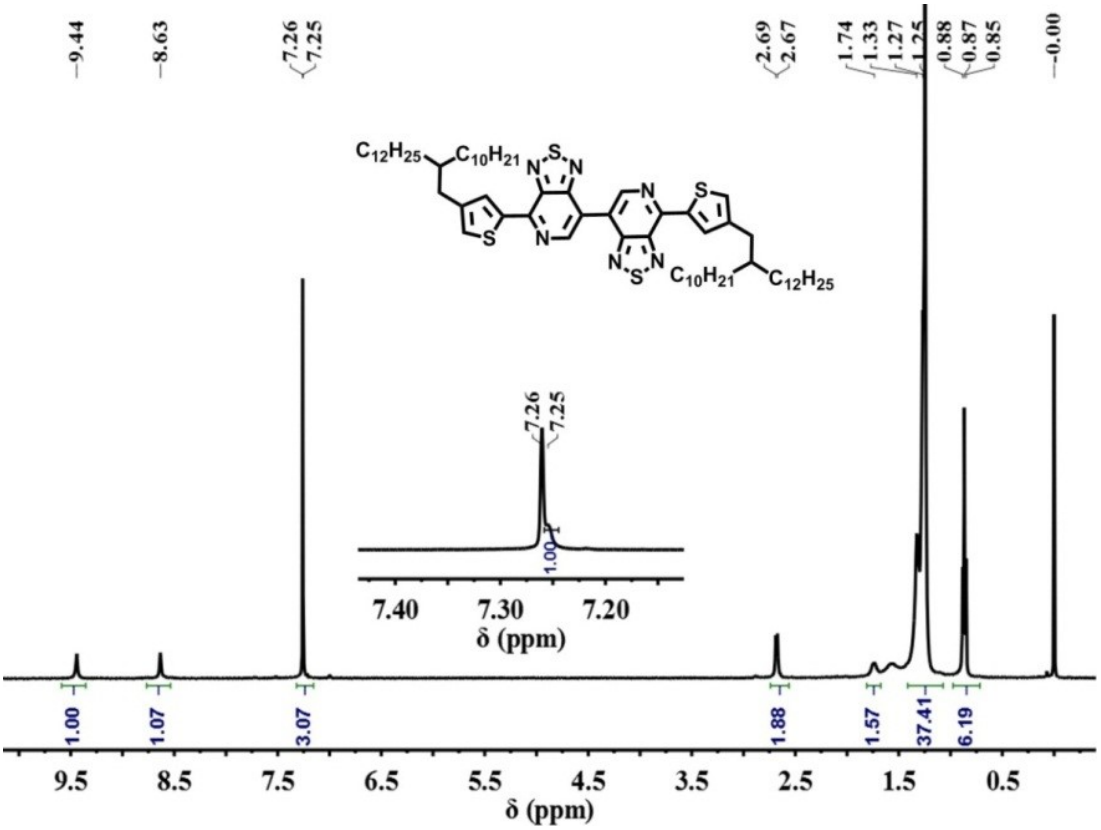

Fig. S13. ^{1}H NMR spectrum of **BPT-T-2** ($CDCl_3$, 25 °C).

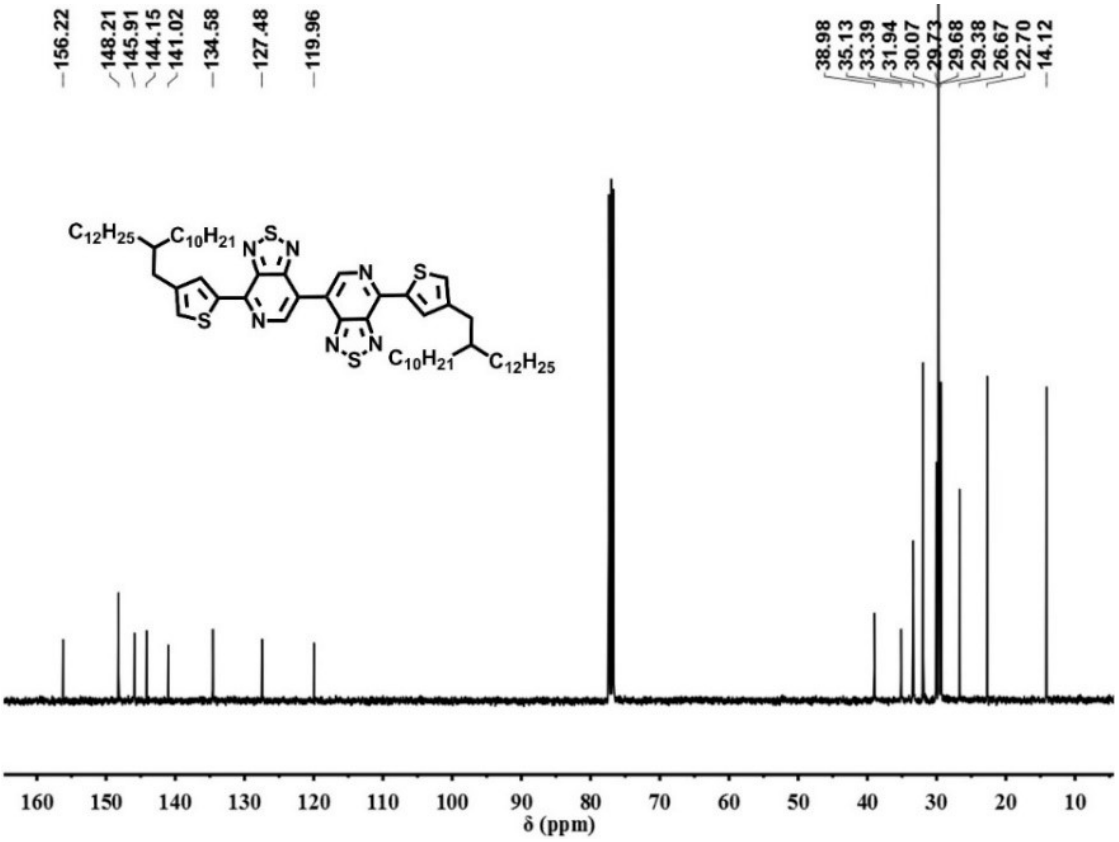

Fig. S14. ^{13}C NMR spectrum of **BPT-T-2** ($CDCl_3$, 25 °C).

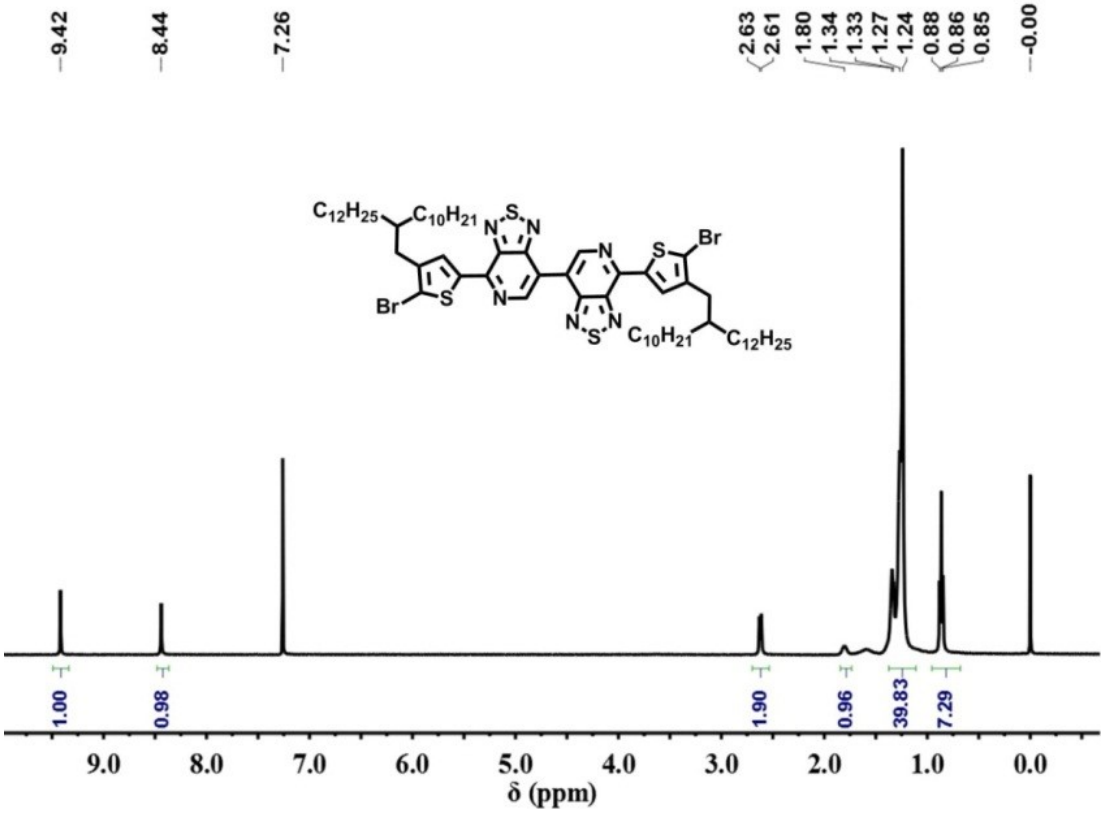

Fig. S15. ^{1}H NMR spectrum of **BPT-2Br** ($CDCl_3$, 25 °C).

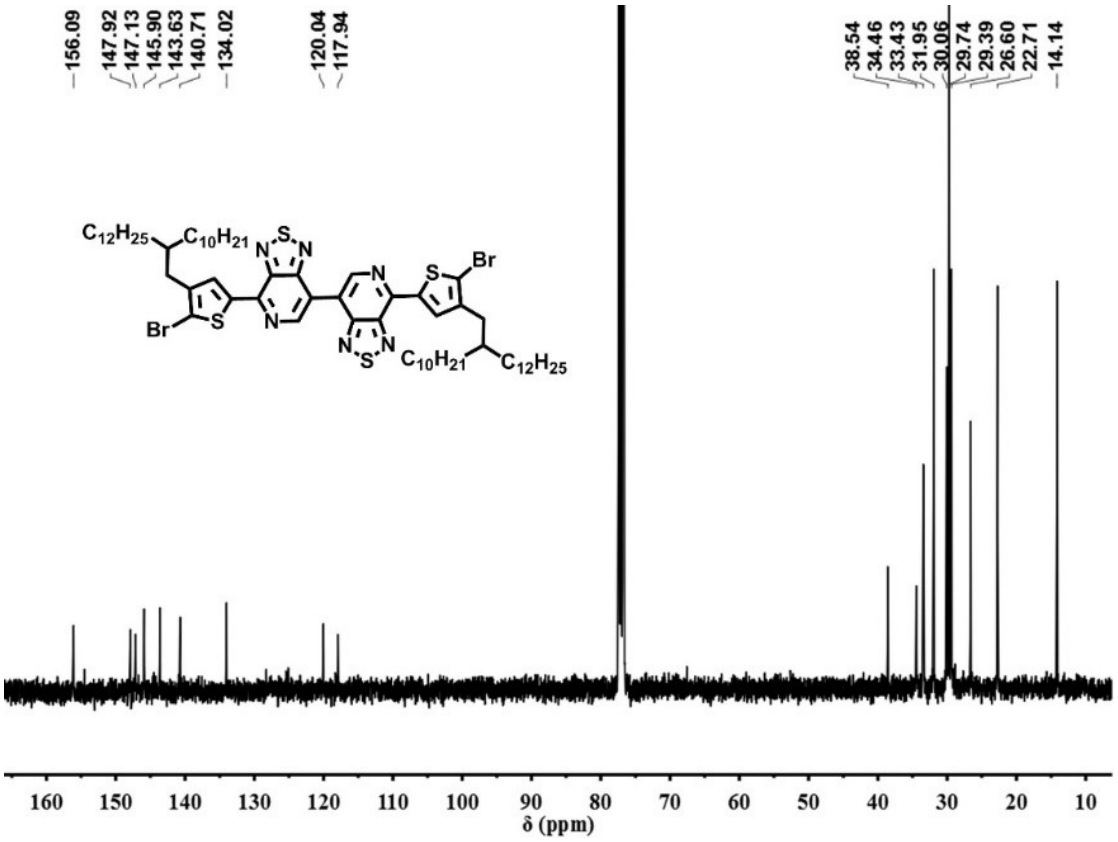

Fig. S16. ^{13}C NMR spectrum of **BPT-2Br** ($CDCl_3$, 25 °C).

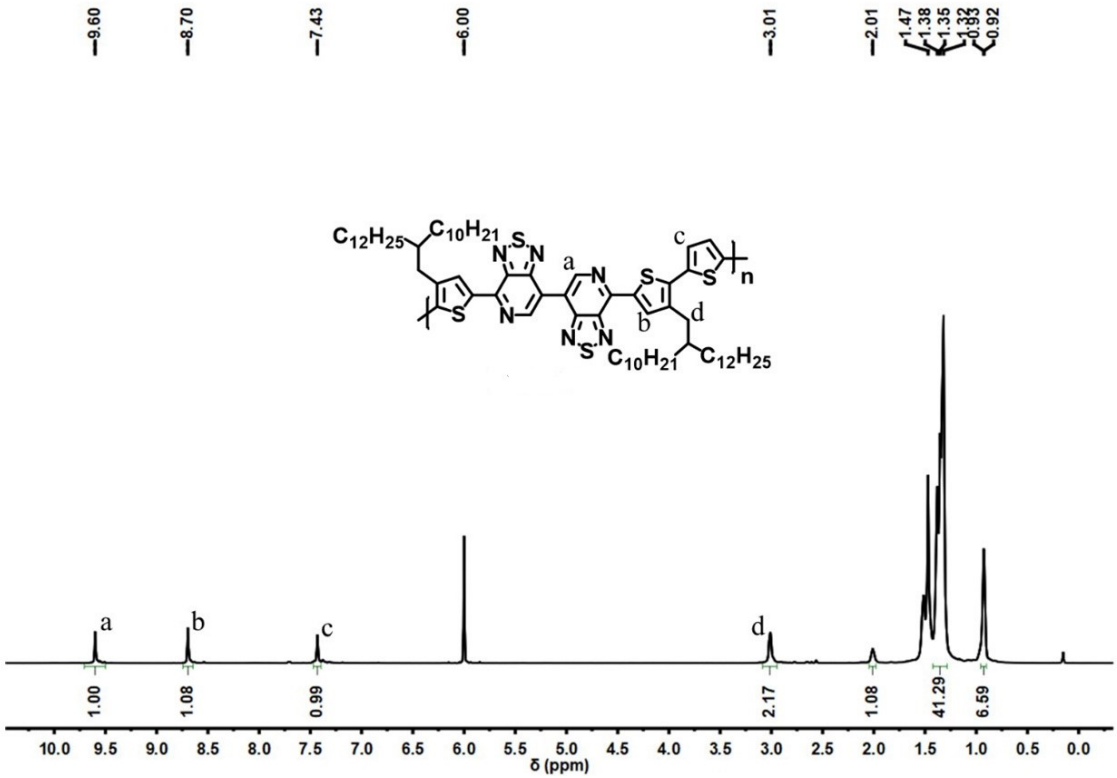

Fig. S17. ^{1}H NMR spectrum of **PBPT-TT** ($C_2Cl_4D_2$, 100 ℃).

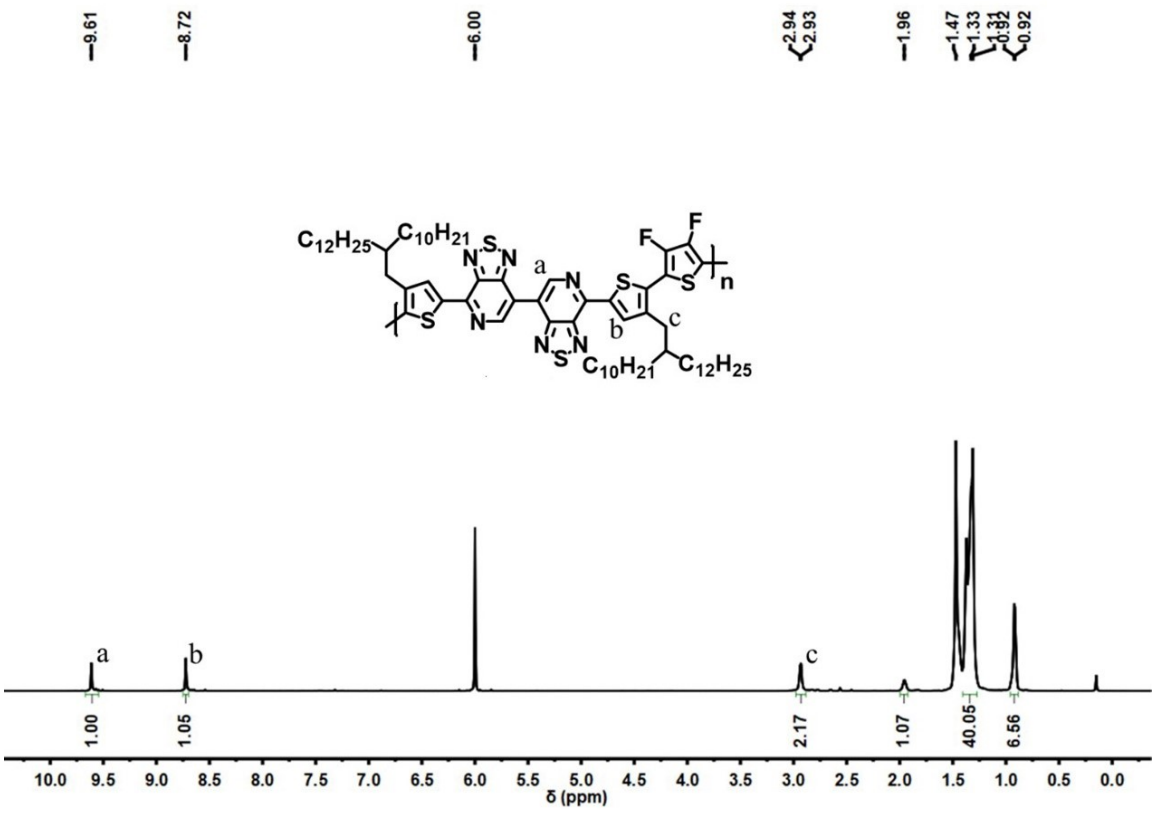

Fig. S18. ^{1}H NMR spectrum of **PBPT-FTT** ($C_2Cl_4D_2$, 100 ℃).

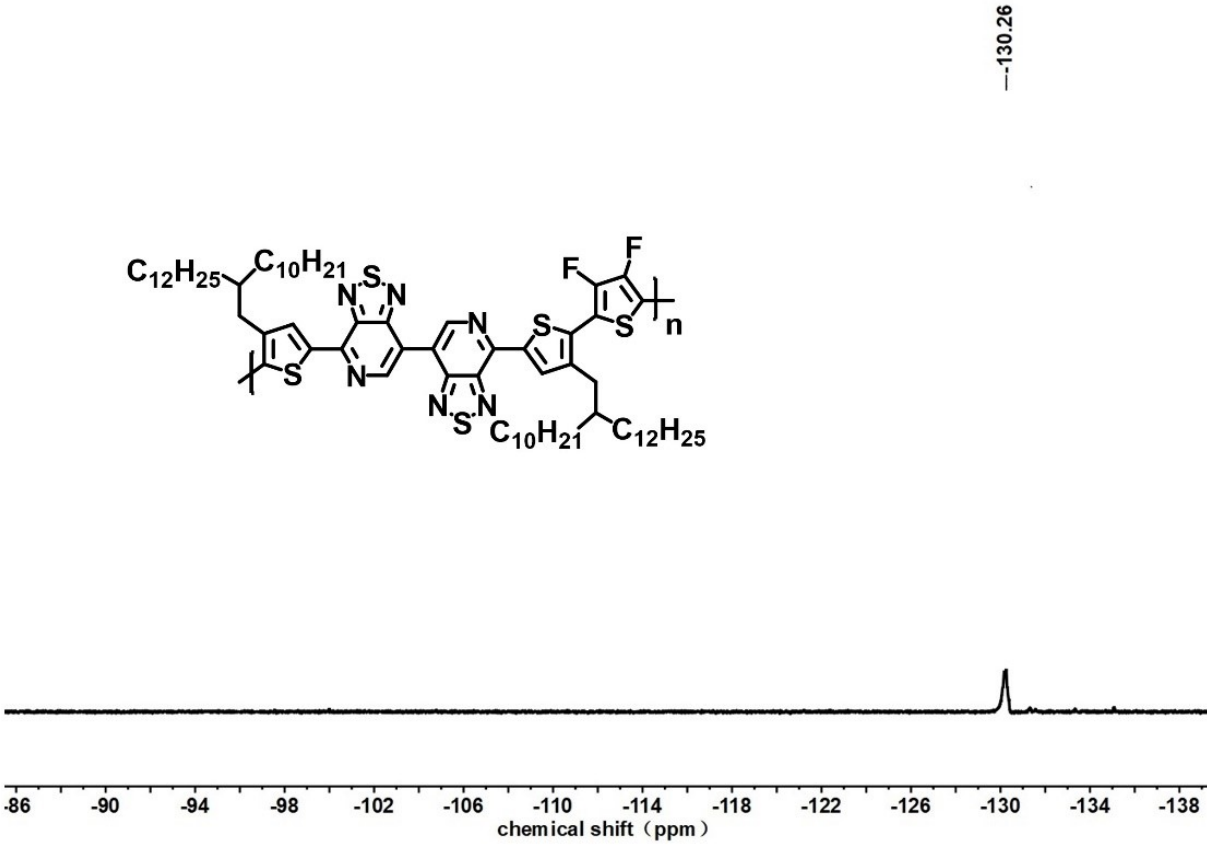

Fig. S19. ^{19}F NMR spectrum of **PBPT-FTT** ($CDCl_3$, 40°C).